Computers and Geotechnics 141 (2022) 104519

Contents lists available at ScienceDirect

Computers and Geotechnics

journal homepage: www.elsevier.com/locate/compgeo

A cyclic p-y model for the whole-life response of piles in soft clay

D.J. White [a,*], J.P. Doherty [b], M. Guevara [b], P.G. Watson [b]

[a] University of Southampton, United Kingdom
[b] University of Western Australia, Australia

ARTICLE INFO

Keywords:
Piles
Soft clay
Lateral loading
Consolidation

ABSTRACT

It is evident from model testing, field studies and theoretical considerations that the strength of a soft clay can reduce and then recover – potentially to above the initial value – as a result of cyclic loading followed by consolidation. For piled foundations and well conductors, these changes in soil strength and the resulting lateral resistance affect their stiffness, capacity and fatigue. This paper introduces a new model for the cyclic lateral '*p-y*' response of a pile in soft clay, using concepts from critical state soil mechanics, combined with a parallel Iwan model to capture the hysteric response. Example analyses show that the model can capture the general forms of behaviour observed in model tests, and is rapid and simple to implement. The model provides a new basis for whole life modelling of piles and well conductors, allowing changes in stiffness and capacity to be simulated, as well as improved modelling of fatigue accumulation. This approach allows more reliable design, quantifying the benefits and risks associated with evolving soil strength.

1. Introduction

Pile foundations and oil and gas well conductors rely on lateral support from the soil to resist horizontal loads. The part of a well conductor immediately below the seafloor acts as a laterally-loaded pile that provides restraint for the well sections below and above. It is conventional for the soil reaction on piles and conductors to be reduced to a single degree of freedom '*p-y*' non-linear spring, which describes the lateral resistance offered by the integrated effect of the soil around the pile. In soft clay, theoretical solutions exist to link the elastic stiffness and plastic strength of the soil to the initial *p-y* stiffness and the limiting resistance, p_u, on the pile, respectively (Baguelin et al. 1977, Randolph and Houlsby 1984). Empirical approaches, calibrated to field tests, have been used to define the full p-y load–displacement response (e.g. Matlock 1970).

It has long been recognised that cyclic loading causes softening of clay due to pore pressure generation, and methods exist to estimate the resulting cyclic strength for design calculations (e.g. Andersen et al. 1988). For laterally-loaded piles, modifications to the monotonic p-y response have been proposed to allow for the effects of cyclic loading, which generally involve a factoring down of the static lateral resistance (e.g. Doyle et al. 2004). A further adjustment for the strain rate during cyclic loading compared to static laboratory tests may compensate for this reduction. Also, more sophisticated methods exist to convert a history of cyclic loading into a specific p-y response (Erbrich et al. 2010, Zhang et al. 2017, Komolafe and Aubeny 2020).

Recent studies have also highlighted that dissipation of the pore pressure generated by undrained cyclic loading leads to reconsolidation and recovery of the soil strength. Model tests of 'episodic' cyclic loading – i.e. with sets of cycles interspersed by periods of consolidation – by Zhang et al. (2011) showed the pile head lateral stiffness fall to 40% of the initial value during an initial cyclic episode, but then rise by a factor of 2 following subsequent consolidation periods. Further results presented by Doherty et al. (2019), Lai et al. (2020) and Guevara et al. (2020) show similar trends in more detail, illustrating the effects of cyclic amplitude, pile length and different patterns of cycling and waiting periods. The observed changes in p-y stiffness are significant and affect the stability, stiffness and fatigue rate of piles and well conductors.

The same process of cyclic softening followed by consolidation and strengthening has been recognised in the behaviour of pipelines, foundation and anchors on soft clay seabeds, and has been captured by simple design-focused models based on critical state soil mechanics (e.g. Boukpeti and White 2017, Cocjin et al. 2017, DNV-GL 2019, Zhou et al. 2020). The purpose of this paper is to outline a model for the lateral p-y response of piles that captures these same underlying mechanisms.

The proposed p-y model consists of two components:

* Corresponding author.
E-mail address: david.white@soton.ac.uk (D.J. White).

https://doi.org/10.1016/j.compgeo.2021.104519
Received 24 May 2021; Received in revised form 24 August 2021; Accepted 12 October 2021
Available online 30 October 2021
0266-352X/© 2021 The Authors. Published by Elsevier Ltd. This is an open access article under the CC BY license (http://creativecommons.org/licenses/by/4.0/).

- A critical state-inspired (CSI) model for hardening and softening of the p-y response
- A parallel Iwan (PI) model (Iwan 1966) for the hysteretic non-linearity of the p-y response

Referred to as the PICSI (parallel Iwan critical state-inspired) model, it tracks the softening caused by lateral pile movement and straining of the surrounding soil, as well as the hardening caused by consolidation over time. The net effect of the softening and hardening varies with time, and is used to scale the strength and stiffness within the PI model of the lateral pile response.

2. CSI model for hardening and softening

2.1. Overview

The PICSI model uses an analogue of the voids ratio – strength relationship that underpins critical state soil mechanics, augmented by a minimum of additional features to replicate model test observations. Voids ratio is replaced with a hardening index, H ($0 < H < 1$), and the mean effective stress is replaced by the undrained strength, s_u (normalised by an initial value, $s_{u,i}$), as illustrated in Fig. 1. $H = 0$ is the initial condition and $H = 1$ is the ultimate limiting condition.

The model represents the behaviour of soil that is initially on the 'wet side' of the critical state, meaning that the soil has a tendency to densify on shearing, eventually reaching a higher undrained strength. Continuous cycling from the initial state results in excess pore pressure that temporarily reduces the undrained strength. The pore pressure effect is captured by a proxy parameter called the damage index, D ($0 < D < 1$). Consolidation causes densification and hardening through the dissipation of pore pressure. This is captured in the model by a time-dependent reduction in damage index concurrent with an increase in hardening index, which is analogous to consolidation following an unload-reload path – we therefore define the slope of this path using κ^*. In the initial state ($H = 0$), the minimum strength is $s_{u,r} = s_{u,i}/S_{t0}$ where S_{t0} is the initial sensitivity. As the soil progressively densifies, the sensitivity reduces to unity. The behaviour therefore converges towards a maximum or final strength, $s_{u,f}$, which is related to $s_{u,i}$ via the parameter λ^*. This parameter is analogous to the slope of the critical state line, which is also linked to the potential change in soil strength from densification, as illustrated by interpretation of the Atterberg limit tests (Wroth and Wood 1978).

In conventional critical state models, there is a single unique (critical state) strength for a given hardening level. In this present model, the soil strength for a particular hardening value is instead bracketed by initial and remoulded values of strengths (an approach proposed previously by White & Hodder (2010), and other subsequent publications). This feature provides a range of potential strengths for any hardening value, rather than a single critical state value, which allows the model to exhibit remoulding and recovery of strength.

The interaction between damage, consolidation and hardening is illustrated in Fig. 1. The three paths labelled A-C represent continuous cyclic loading at different rates relative to the consolidation process are identified to show the potential ways that the undrained strength can evolve. The 'fast' case A involves negligible consolidation, so the strength simply falls from the initial to the remoulded value, as observed in cyclic T-bar tests and cyclic lateral pile tests in which negligible consolidation occurs (e.g. Stewart and Randolph 1991, Doyle et al. 2004). The 'slow' case C involves a high level of consolidation between each cycle or shearing stage, so the effect of consolidation and hardening eclipses the generation of pore pressure and softening. As a result, the strength rises with every cycle, converging towards the limit. The same behaviour has been observed in axial pipe-seabed sliding tests (Smith and White 2014), interface shear box tests (Boukpeti and White 2017) and episodic T-bar penetrometer tests (Cocjin et al. 2014). However, we are not aware of any lateral pile tests in soft clay that have been conducted with sufficient consolidation between cycles to match this trend. Case B represents continuous cycling at a rate that is intermediate between A and C.

Case E represents episodic cycling, in which packets of fast cycles are interspersed with periods of consolidation. In this case, the softening during each cyclic period is followed by hardening, as the effect of pore pressure dissipation eclipses the effect of generation. The net result is a rise in strength and stiffness, and a reduction in the sensitivity observed in each packet. This trend matches published results from various model testing studies of lateral pile behaviour (Zhang et al. 2011, Doherty et al. 2019, Guevara et al. 2020, Lai et al. 2020) as well as analogous studies of cyclic T-bar penetrometer tests (White & Hodder 2010) or plate anchor loading (Zhou et al. 2020).

2.2. Governing equations

2.2.1. Current strength

The current normalised strength, $s_u/s_{u,i}$, depends on the current hardening, H, and damage, D. An equilibrated strength, $s_{u,e}$ is defined as the strength at the current H when $D = 0$ (Eq. (1)):

$$\frac{s_{u,e}}{s_{u,i}} = 1 + \frac{H}{\lambda^*} \tag{1}$$

The current strength, s_u, is therefore:

$$\frac{s_u}{s_{u,e}} = 1 - D\left(1 - \frac{1}{S_t}\right) \tag{2}$$

A general form of the geometry of the model (Fig. 1) allows the sensitivity to fall with the hardening, from $S_t = S_{t0}$ at $H = 0$ to $S_t = 1$ at $H = 1$, at a rate set by the power, q:

$$S_t = 1 + (S_{t0} - 1)(1 - H)^q \tag{3}$$

This tendency for the sensitivity of a sample to diminish through repeated episodes of cyclic shearing and consolidation has been observed in T-bar penetrometer tests (Hodder et al. 2009) – which are analogous to large-amplitude lateral pile motion – and also during cyclic lateral loading of piles (Zhang et al. 2011). This trend of S_t given by Eq. (3) can be interpreted as there being no tendency for pore pressure to be generated once $H = 1$, because the soil is at a critical state under the equilibrated effective stress (i.e. when $D = 0$). The sensitivity therefore falls to 1 and the damage and hardening processes stop.

In an initial burst of cyclic loading, taking place over a short time so that consolidation and hardening is minimal (i.e. $H = 0$), the strength changes from an initial value ($s_u = s_{u,i}$) as damage accumulates ($D \to 1$) so that $s_u \to s_{u,r}$. In the long term, as consolidation dominates, $H \to 1$ so $s_u \to s_{u,f}$, so long as there is cyclic motion that leads to damage, from which consolidation can create the gain in strength (see Fig. 1 for the strength notation).

2.2.2. Generation of damage

The damage is caused by shearing of the surrounding soil during changes in normalised lateral pile position, y/d (where d is the pile diameter), and cannot exceed $D = 1$. A simple function to describe this behaviour is:

$$\delta D = d_r(1 - D)^{d_p}\left|\frac{y}{y_{ref}}\right|^{d_a}\left|\frac{\delta y}{d}\right| \tag{4}$$

where d_r and d_p are dimensionless constants representing the damage rate and power coefficients, while $\delta y/d$ is a normalised displacement increment. The term $\left|\frac{y}{y_{ref}}\right|^{d_a}$ allows the rate of damage to depend on the amplitude of displacement, and not just the cumulative displacement, controlled by the exponent d_a. The parameter y_{ref} is a reference displacement introduced to make this term dimensionless and should be

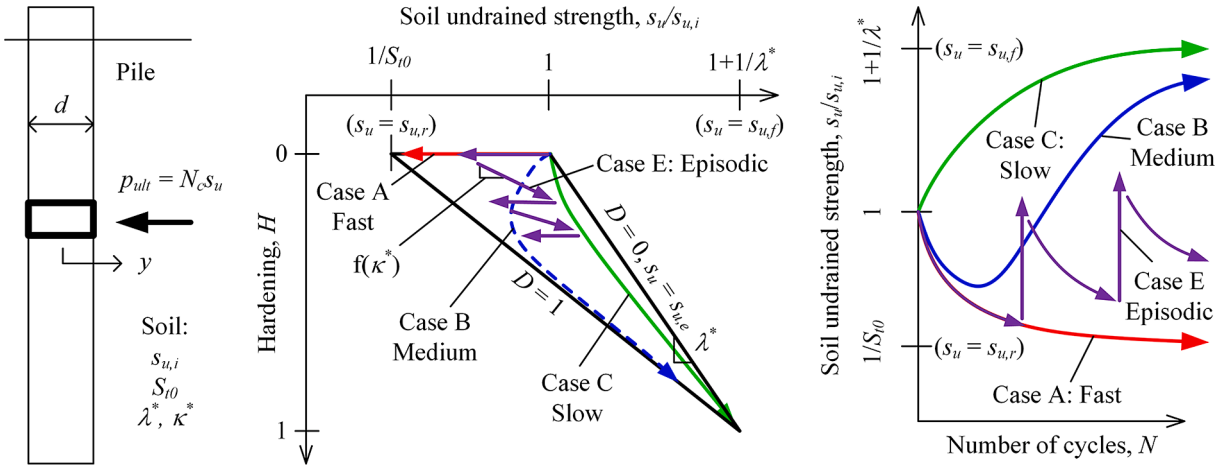

Fig. 1. Illustration of model notation and parameters.

defined as a fraction of the pile diameter, so that consistent parameters can be used across a range of pile sizes[1]. For the case of $d_a = 0$, Eq. (4) can be integrated to show that, for a given d_p, the damage is a function of the scaled cumulative normalised lateral displacement Sd_r, where $S = \Sigma|\delta y/d|$. By including d_r in this scaled displacement, responses for soils with different damage rates (or levels of 'brittleness') will coincide. This behaviour is shown in Fig. 2, for a range of values of the damage rate parameter, d_p.

Two practical illustrations are used to highlight this approach:

- Firstly, the degradation in lateral stiffness observed by (Zhang et al. 2011) during lateral undrained cycles of a model pile in kaolin clay is plotted on Fig. 2. These stiffness values are the secant peak-to-peak stiffness within a cycle, $K = \delta F_h/y^{pp}$ where δF_h is the difference between the peak values of horizontal force at each cyclic limit and y^{pp} is the pile displacement between these peak values of F_h. The values of K are scaled so that initial and the steady final stiffnesses correspond to $D = 0$ and 1 respectively. This trend corresponds to $d_p \sim 2$ for $d_r = 1$.
- Cyclic T-bar penetrometer tests provide a second comparison, being analogous to cyclic lateral pile loading. The cycle-by-cycle degradation of steady penetration resistance observed in cyclic T-bar penetrometer tests in soft clay agrees well with the damage function for $d_p \sim 1$–2 for $d_r \sim 1$, as shown on Fig. 2. This comparison uses the numerical simulations of Zhou and Randolph (2009), which showed that the failure mechanism around the T-bar has an extent in the direction of movement of approximately two diameters. On this basis, a single pass of the T-bar causes strain in the soil that is equivalent to two diameters of T-bar or pile movement. During the first pass, the average accumulated strain corresponds to one diameter, and during the return pass the average strain therefore corresponds to three diameters. The response marked on Fig. 2 is based on a strain of 10–20 being required for 95% of full remoulding, which originates from interpretation of cyclic T-bar penetrometer data (Randolph 2004, Zhou and Randolph 2009).

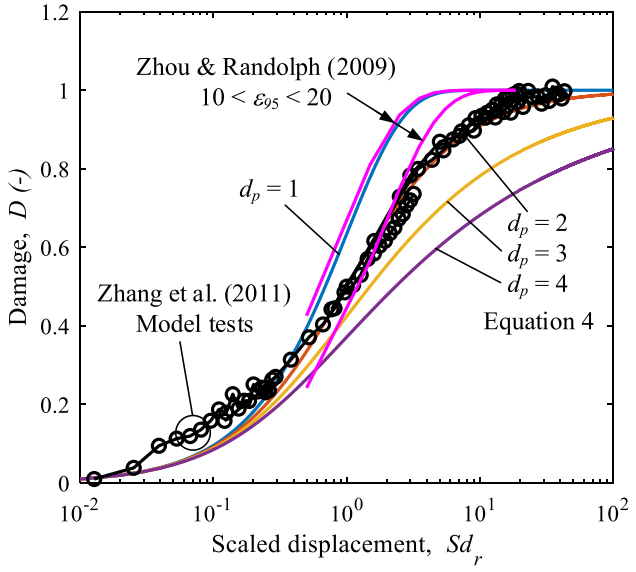

Fig. 2. Damage as a function of the scaled cumulative displacement (for $d_a = 0$).

[1] Subsequent examples in this paper assume $d_a = 0$, so the parameter y_{ref} is not used.

This formulation does not recognise cyclic loading as being more damaging than monotonic loading to the same accumulated deformation, which is a limitation that is tolerated in other practical models for soil softening (e.g. Whyte et al. 2020). More complex alternatives could be used in place of Eq. (4), based on other established models for pore pressure build up during cyclic loading.

2.2.3. Dissipation of damage

The damage decays with time due to pore pressure dissipation, leading to consolidation. The time rate of this decay follows the usual scaling of consolidation, being proportional to c_v/d^2:

$$\frac{\delta D}{\delta t} = -c_r\left(\frac{c_v}{d^2}\right)D^{c_p} \tag{5}$$

where c_r and c_p are dimensionless parameters controlling the rate and power of this consolidation effect respectively. Fig. 3 plots D, obtained by integrating Eq. (5) from an initial $D = 1$, against dimensionless time T, where $T = c_v t/d^2$ for a range of c_p values. The parameters give the solution flexibility to be scaled to match analytical solutions for the dissipation of pore pressures around a laterally loaded pile.

The resulting consolidation process is compared in Fig. 3 with the dissipation solution by Osman and Randolph (2012), using Eq. (5) integrated with $c_r = 5$, for a range of c_p values. It can be seen that $c_p = 3$ provides a reasonable match. However, this comparison relates to consolidation in response to sustained monotonic loading.

Combining Eqs. (4) and (5), the general variation of damage is:

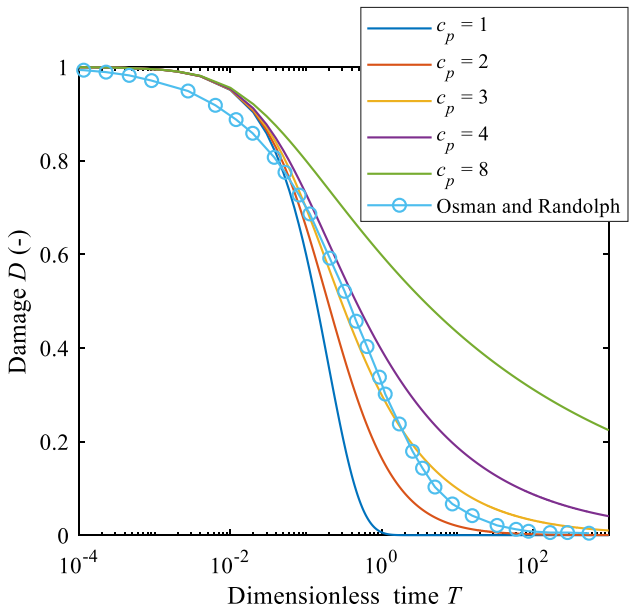

Fig. 3. Damage recovery as a function of the dimensionless time for $c_r = 5$, compared with the consolidation solution of Osman and Randolph (2012).

$$\delta D = d_r(1-D)^{d_p}\left|\frac{\delta y}{d}\right|\left|\frac{y}{y_f}\right|^{d_a} - c_r\left(\frac{c_v}{d^2}\right)D^{c_p}\delta t \tag{6}$$

Comparing Fig. 2 and Fig. 3 it is evident that the accumulation of damage from $D = 0$ and the decay of damage from $D = 1$ are controlled by the scaled dimensionless cumulative displacement (Sd_r) and the scaled dimensionless time (Tc_r) in exactly the same way. Therefore, for a fixed set of constants, the combined response in Eq. (6) is a function of the scaled dimensionless pile velocity (Eq. (7)), which controls the distance travelled per unit time, and therefore the relative rates of damage and hardening:

$$V = \frac{Sd_r}{Tc_r} \tag{7}$$

This relationship is demonstrated in Fig. 4, which shows the development of damage with scaled distance (or time) for $d_r = 1$, $c_r = 5$ and $d_p = c_p = 3$. All responses stabilise at a constant damage that increases with

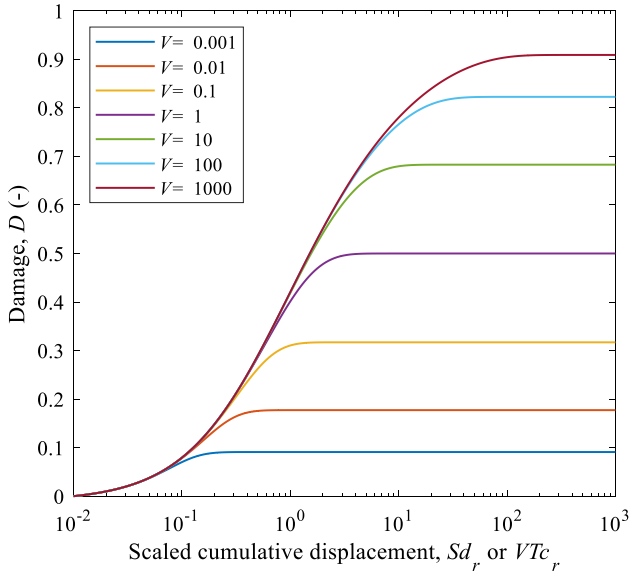

Fig. 4. Damage accumulation during steady motion at different rates.

scaled dimensionless pile velocity. This reflects that at higher velocities there is greater generation, and so a higher damage level is sustained in balance with the dissipation.

2.2.4. Evolution of hardening

Consolidation leads to hardening, following a path in the $H - s_u/s_{u,i}$ plane dependent on κ^* (see Fig. 1). When the pile is stationary (i.e. $\frac{\delta y}{\delta t} = 0$), $\frac{\delta H}{\delta D} = -\kappa^*(1-H)^{h_p}$. This formulation means that κ^* sets the initial slope of the hardening response at $H = 0$, and lies in the range 0 to 1. The power coefficient h_p sets how this slope changes as the limit of $H = 1$ is approached. Modifying Eq. (5), the hardening evolution can be written as:

$$\frac{\delta H}{\delta t} = c_r(1-H)^{h_p}\left(\frac{\kappa^* c_v}{d^2}\right)D^{c_p} \tag{8}$$

As for the damage model, a minimal number of parameters are used.

To illustrate the hardening model, the variation of H and $s_u/s_{u,i}$ with time is shown in Fig. 5 using the same range of parameters as used in Fig. 4 ($\lambda^* = 0.5$, $\kappa^* = 0.5$, $h_p = 2$ and $S_{t0} = 5$). In all cases, the strength evolves towards the limit of $s_{u,f}$, but for movement that is more rapid relative to dissipation, there is a fall in strength associated with undrained cyclic loading and pore pressure generation.

2.2.5. Illustration of typical model responses

To illustrate the model response, we firstly present a simulation of the changing strength around a pile during episodic loading (Fig. 6). In this example, a 1 m diameter pile is first subject to 50 cycles of normalised amplitude $\delta y/d = \pm 0.1$, thereby moving by a scaled distance of $Sd_r = 20$ diameters with $d_r = 1$. Adopting a 10 s cyclic period, the corresponding dimensionless velocity is $V > 25{,}000$ and the 50 cycles take a dimensionless time of $T < 2 \times 10^{-4}$. The pile is then stationary for a period of $T = 3.17$, while consolidation occurs, corresponding to 107 s (or 116 days) in soil with $c_v = 10$ m^2/year. The sequence of cycling and recovery is repeated 5 times. The other model parameters adopted are the same as in Fig. 5.

The time histories of progressive hardening and repeated damage and consolidation are shown in Fig. 6a to c. The hardening-strength path is shown in Fig. 6d, bounded by the limits of $D = 0$ and $D = 1$. The resulting evolution of soil strength is shown in Fig. 6e.

This example is a highly idealised representation of the changing excitation that a pile or well conductor might experience. However, it shows that the model can capture general patterns of changing strength, associated with arbitrary sequences of movement and damage coupled with ongoing consolidation.

In a second example (see Fig. 7), the model is compared with the strength response from an episodic cyclic T-bar penetrometer test (White & Hodder 2010), with the cylindrical T-bar being comparable to an element of pile. The soil disturbance from each passing of the T-bar is represented by two diameters of pile movement. After each packet of 20 cycles, the T-bar is held stationary and consolidation occurs. The model replicates the test data well, and also matches closely the CSI cycle-by-cycle strength model presented in the same study, which has a similar basis. A distinction between the two models is that in the White & Hodder (2010) model the smallest increment of damage corresponds to a T-bar cycle, whereas the present model is formulated in terms of pile (or T-bar) displacement, and therefore can be applied to general patterns of movement via the PI model, which is described in the next section.

3. Parallel Iwan (PI) model for non-linear cyclic P-Y response

3.1. Overview

The PICSI model tracks the softening and hardening behaviour of the soil surrounding the pile, and then uses this to scale the p-y response. This response is formed of parallel Iwan elements (Iwan 1966). These

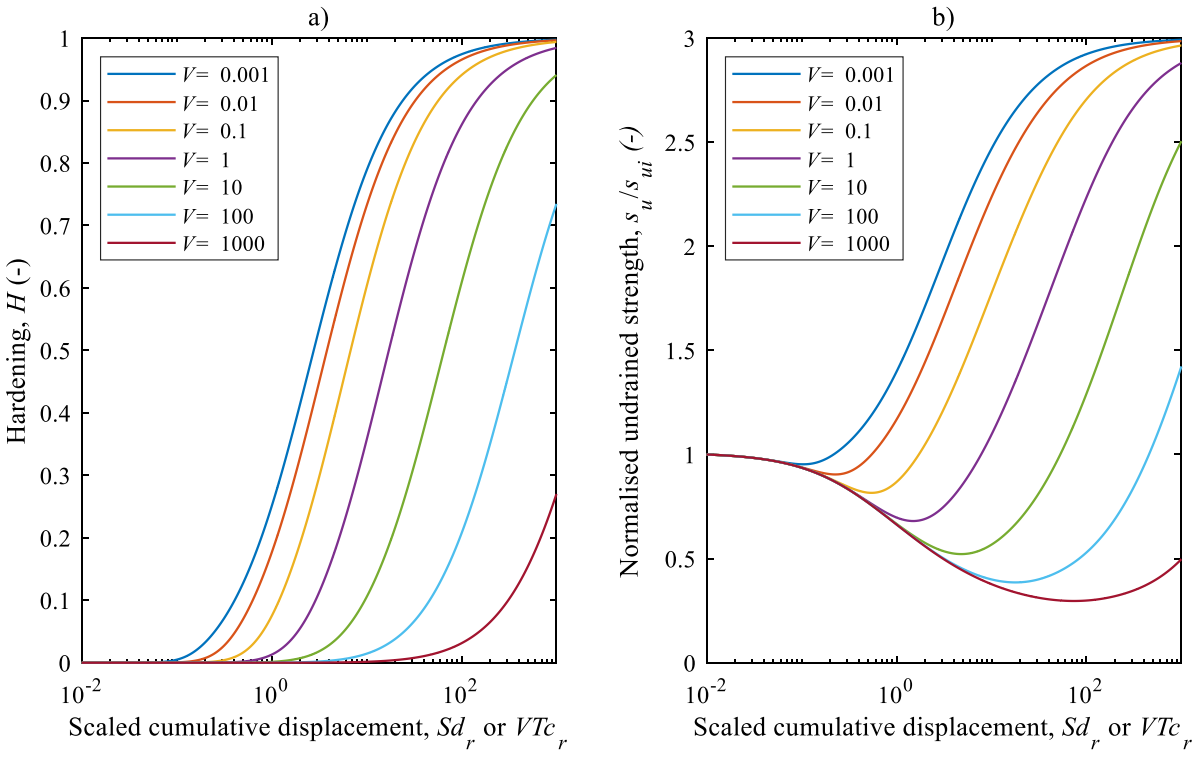

Fig. 5. Hardening and strength changes during steady motion.

elements allow general forms of cyclic behaviour to be captured, including features such as the non-linearity of the monotonic and cyclic responses with high stiffness at reversal points and a progressive reduction in tangent stiffness as the limiting resistance is approached. A parallel Iwan (PI) model consists of a number of spring-slider elements, each carrying force f_i, with different slider capacities (s_i) and spring stiffness values (k_i) (Fig. 8). PI models have been used previously to describe the p-y response of piles (e.g. Einav 2005, Beuckelaers 2015) and the contribution of this paper is to couple the PI and CSI models to capture softening and hardening observed in cyclic loading of piles. In this paper p represents the lateral force per unit length of pile, which has typical units of kN/m, such that p/d is the net lateral pressure on the pile.

3.2. Conversion of monotonic backbone curve to PI model parameters

For a monotonic loading event, the PICSI model should reproduce a specified monotonic "backbone" curve. It is therefore convenient to work backwards from a monotonic p-y curve to derive the stiffness of each of the parallel springs (k_i) and the capacity of the sliders (s_i). To do this a backbone curve is first discretised as shown in Fig. 9.

Values for p_0 to p_n and y_0 to y_n are then known. The tangent stiffness of each segment (E_i) of the backbone curve can be computed as (Eq. (9)):

$$E_i = \frac{p_i - p_{i-1}}{y_i - y_{i-1}} \quad i = 1 \cdots\cdots n \tag{9}$$

The tangent stiffness can also be expressed as the sum of all the active parallel springs, which is

$$E_i = \sum_{j=i}^{n} k_j \tag{10}$$

and Eq. (10) can be written in matrix from as

$$\{E\} = [A]\{k\} \tag{11}$$

where A is an n by n transformation matrix with 1 s on and above the diagonal and zeros below. Values for k for Eq. (11) can then be found using Eq. (12):

$$\{k\} = [A]^{-1}\{E\} \tag{12}$$

The following relationship, Eq. (13), can then be used to find the slider capacities.

$$p_i = \sum_{j=1}^{i} s_j + y_i \sum_{j=i+1}^{n} k_j \tag{13}$$

A second n by n transformation matrix B can be introduced containing 1 s above the diagonal and zeros on and below the diagonal. Eq. (13) can be written in terms of the two matrices

$$\{p\} = [A]^T\{s\} + \{y\}[B]\{k\} \tag{14}$$

where the dot multiplication is used to indicate element by element multiplication of vectors, rather than vector multiplication. Eq. (14) can be rearranged into Eq. (15) to solve for slider capacities

$$\{s\} = [[A]^T]^{-1}\{\{p\} - \{y\}[B]\{k\}\} \tag{15}$$

With the PI parameters (k_n and s_n) derived from the monotonic backbone curve, the model can be implemented by noting that the force in any spring (f_i) is the product of the elastic displacement (u_e) and the spring stiffness (k_i) (Eq. (16)):

$$f_i = k_i u_i^e \tag{16}$$

The elastic displacement is the difference between the total displacement and the plastic displacement (u_i^p) (Eq. (17)).

$$f_i = k_i(y - u_i^p) \tag{17}$$

If

$$abs(f_i) > s_i \tag{18}$$

then Eq. (18) shows that the capacity of the slider has been exceeded and the value of the plastic displacement must be incremented by the change in total displacement. Noting that the maximum elastic displacement in

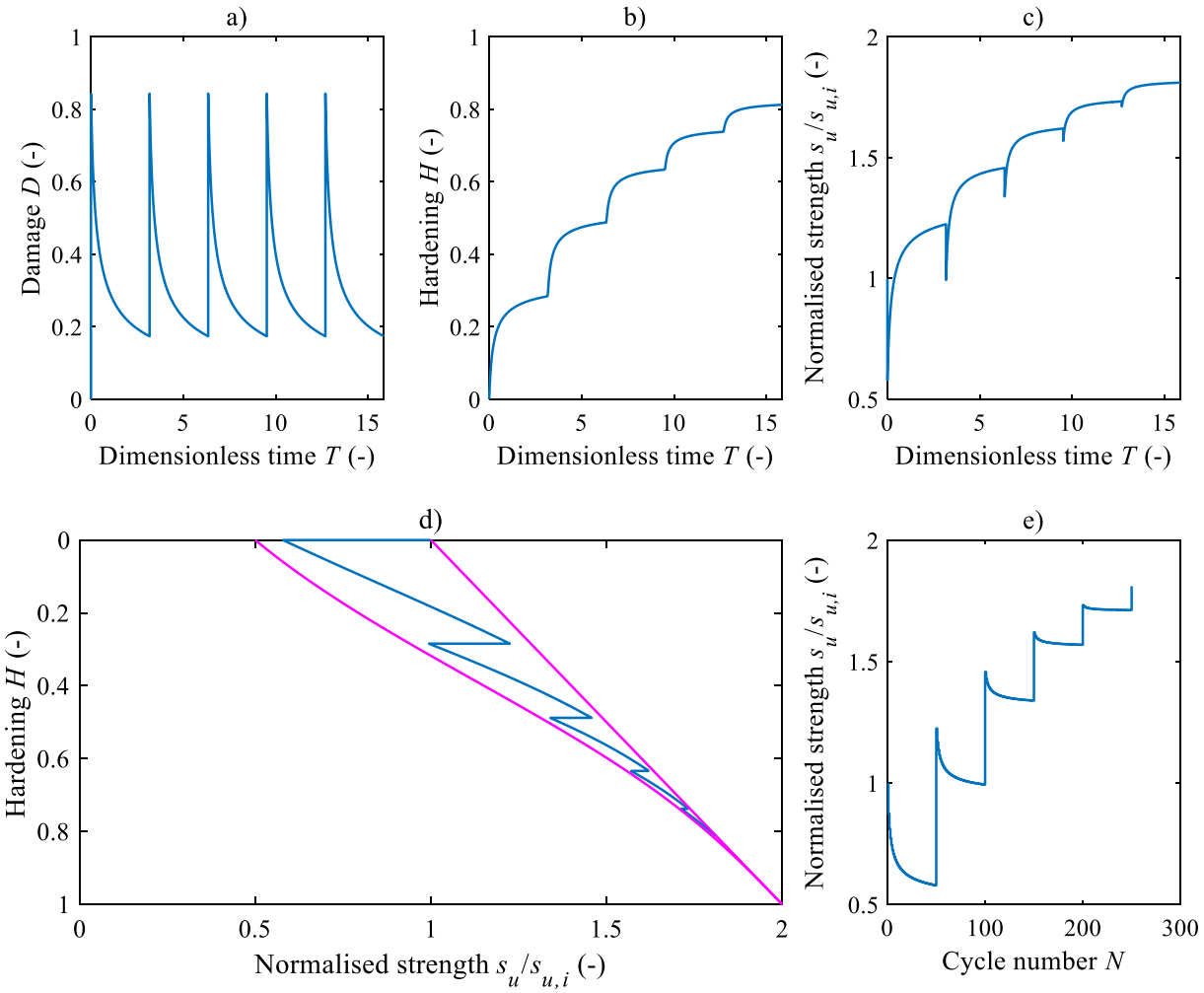

Fig. 6. Example of episodic cyclic motion: Time histories of (a) damage, (b) hardening history and (c) strength; (d) hardening-strength path and (e) cyclic evolution of strength.

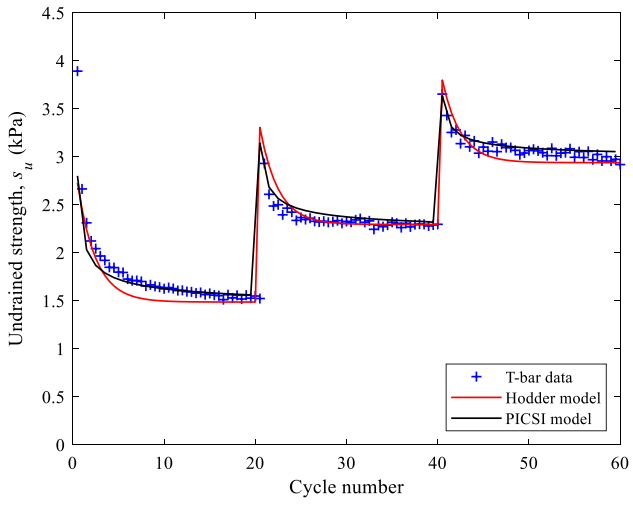

Fig. 7. Comparison with episodic cyclic strength response in penetrometer test.

the spring is s_i/k_i, then the plastic displacement is given by Eq. (19):

$$u_i^p = y \pm \frac{s_i}{k_i} \tag{19}$$

As an example, the Fig. 10 shows the API soft clay p-y curve (API 2011, ISO 2016) discretised with 5 points and the corresponding PI model with 5 springs/slider elements subject to 2-way cyclic loading. There is no cyclic degradation in the base PI model and the CSI model is used to represent the degradation and recovery responses observed in model tests.

3.3. Combining the CSI and PI models

Houlsby et al. (2017) derived a PI ratcheting model within the hyperplastic framework and demonstrated that values of s_n may be varied as functions of the state of the material, without affecting the model formulation. Similarly, to accommodate the changes in strength, and consequently stiffness, the CSI model was linked to the PI response by scaling in the initial slider and spring capacities by the ratio of the current strength to the initial strength:

$$\{s\} = \{s_i\}\frac{s_u}{s_{u,i}} \quad \{k\} = \{k_i\}\frac{s_u}{s_{u,i}} \tag{20}$$

This approach assumes that changes in stiffness mirror changes in strength, with both being adjusted from their initial values by the same proportion. However, the two may not be equally affected for all amplitudes of cyclic loading, depending on the underlying micro-mechanical phenomenon. The model could be extended to have independent scaling approaches to stiffness and strength, seperating the expressions in Eq. (20), if further observations indicate that this is required. However, as shown by later examples, this approach is

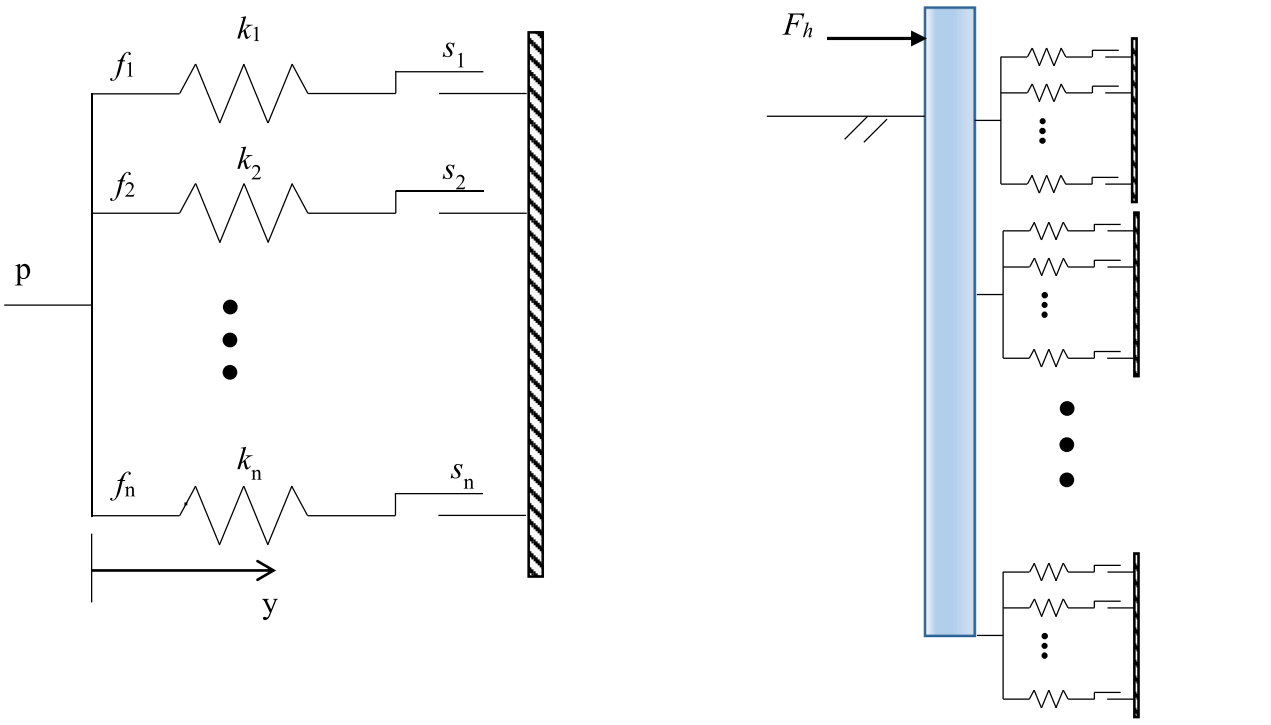

Fig. 8. Parallel Iwan (PI) model and full pile system.

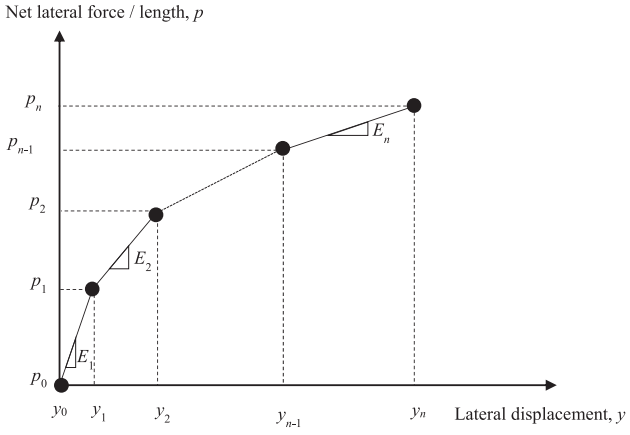

Fig. 9. Discretisation of a p-y backbone curve.

successful based on the data presented in this paper.

4. Example application of PICSI model

A centrifuge model test is used to illustrate the capability of the PICSI model to represent typical observations of lateral pile behaviour. Guevara et al. (2020) present centrifuge test results from a rigid length of pile (or conductor) installed in reconstituted carbonate silt. The pile had a diameter d = 19.5 mm and an embedded length 4.5d, with testing taking place at a g-level of 40. The pile was fixed against rotation and practically rigid for the range of loads applied.

Two tests are considered. In the first test, the pile was subjected to a one-way undrained monotonic push to the ultimate capacity, as shown in Fig. 11. The rigid lateral translation of a pile can be represented with a single PI spring in an F_h-y model, where F_h is the total horizontal force (i.e. the integral of p down the length of the pile). To apply the PI model, the measured monotonic lateral response of the pile was discretized and used to evaluate spring stiffness and slider capacity values for the PI

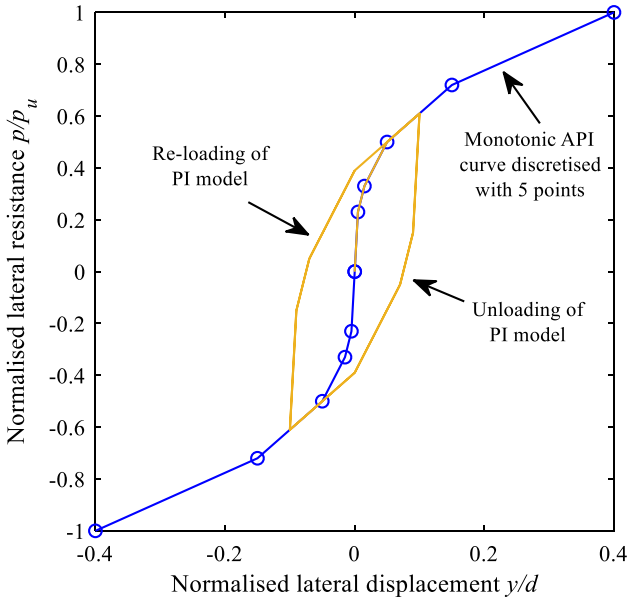

Fig. 10. Example of PI model calibrated to API backbone curve.

model, using the method described above. As shown in Fig. 11, this approach provides an accurate representation of the monotonic behaviour.

The reconstituted carbonate silt used during the centrifuge tests had a measured strength profile of $s_u = 1.65z$ kPa/m, where z is the depth below the soil surface. Using the approach presented by Jeanjean et al. (2017), and averaging the lateral bearing factor, N_p, over the embedded length of the pile (so that $N_p = 11.8$, following Jeanjean et al. 2017), the predicted ultimate capacity is 61.5 N. The load reached in the monotonic test is 65.5 N, which is within 7% of the predicted ultimate capacity.

In the second test, the pile was subjected to cycles of displacement-controlled lateral movement with an approximate normalised

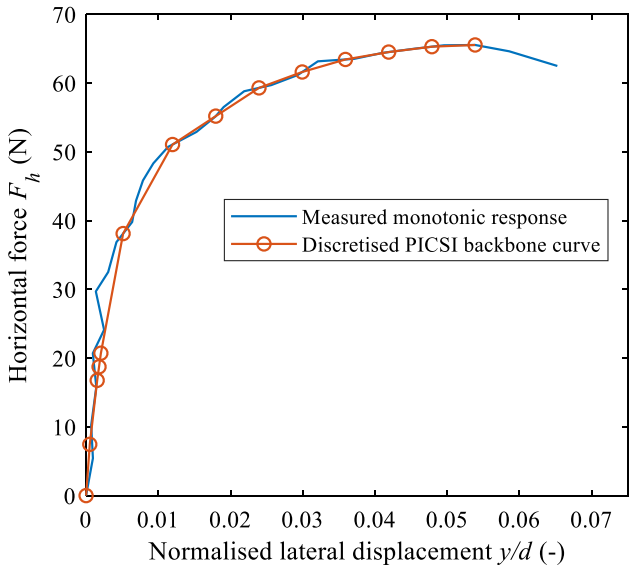

Fig. 11. Centrifuge test comparison: Discretisation of monotonic backbone data.

amplitude of $\delta y/d = \pm 0.04$, at a frequency of $f = 0.625$ Hz. The measured displacement is shown in Fig. 12, and was used as an input into the PICSI analysis, from which the resulting resistance is calculated. During the initial 500 cycles the stiffness fell, with a minimum peak-to-peak secant stiffness ($K = \delta F_h / y^{pp}$) of around 7% of the initial peak-to-peak secant stiffness (K_0). By the end of the test, after 10,000 cycles, the stiffness had increased by a factor of two from this softened minimum value.

To simulate this cyclic test, the PICSI model is overlain on the monotonic PI response of Fig. 11, to capture the changing soil strength and stiffness. The parameter values are listed in Table 1 and are based on the theoretical consideration given earlier in the paper, with minor modifications to improve the match with the experimental data. The adopted initial sensitivity, S_{t0}, is from cyclic T-bar testing of carbonate silt reported by Zhou et al. (2020). The predicted evolution of cyclic secant stiffness is shown in Fig. 13 and the full cyclic response is shown in Fig. 14, compared with the monotonic backbone curve, with key cycles are highlighted. The predicted secant stiffness variation and the overall cyclic response agree well with the experimental data.

5. Discussion

The PICSI model provides a first attempt to capture the complex patterns of changing strength around a pile within a model that can be integrated into a pile response analysis. PI models are increasingly used

Table 1
PICSI model parameters and values for simulation of centrifuge model tests.

Model feature	Parameter		Value
Monotonic response	PI element fitted to monotonic test (Fig. 11)		
Cyclic response:			
Strength limits (Eqs. (1), (2))	Initial sensitivity	S_{t0}	5
	Slope of $D = 0$ line (Fig. 1)	λ^*	0.5
	Effect of hardening on sensitivity	q	1
Damage generation (Eq. (4))	Rate constant	d_r	1.1
	Power constant	d_p	2.3
	Effect of amplitude	d_a	0
Consolidation (Eq. (5))	Consolidation coefficient	c_v	1 m^2/year
	Rate constant	c_r	0.2
	Power constant	c_p	3
Hardening (Eq. (8))	Slope of hardening path (Fig. 1)	κ^*	0.5
	Variation of hardening slope	h_p	1

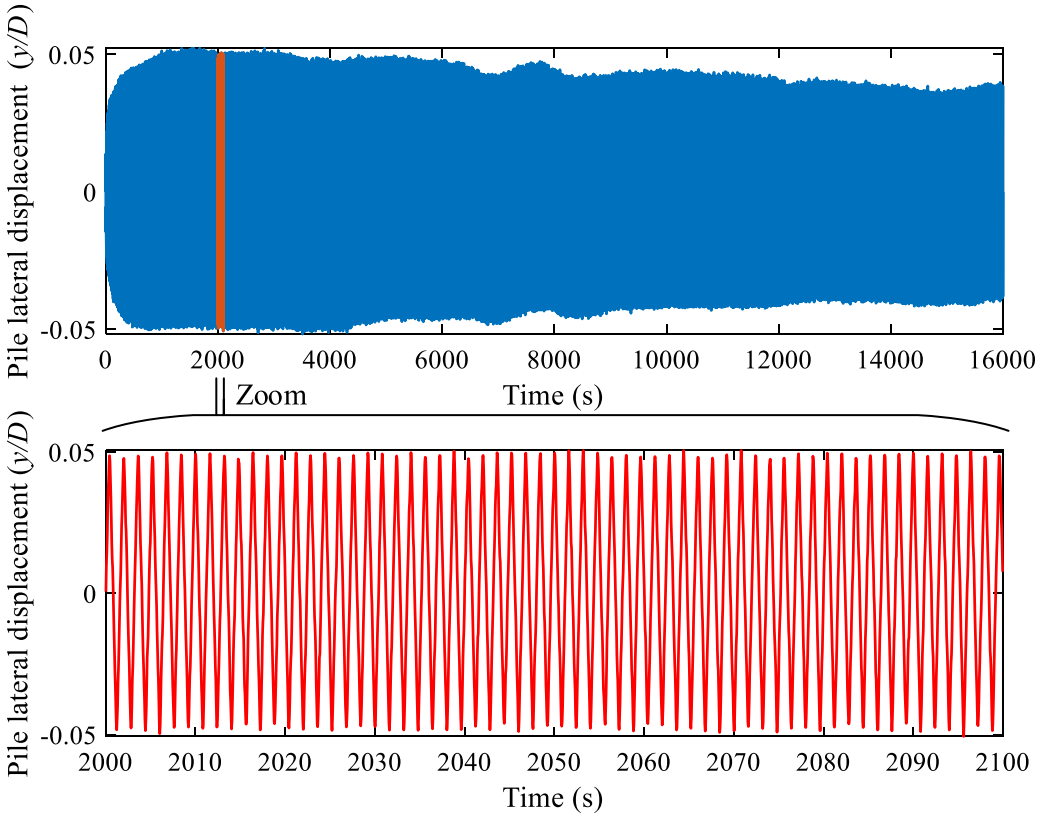

Fig. 12. Measured lateral displacement of model pile.

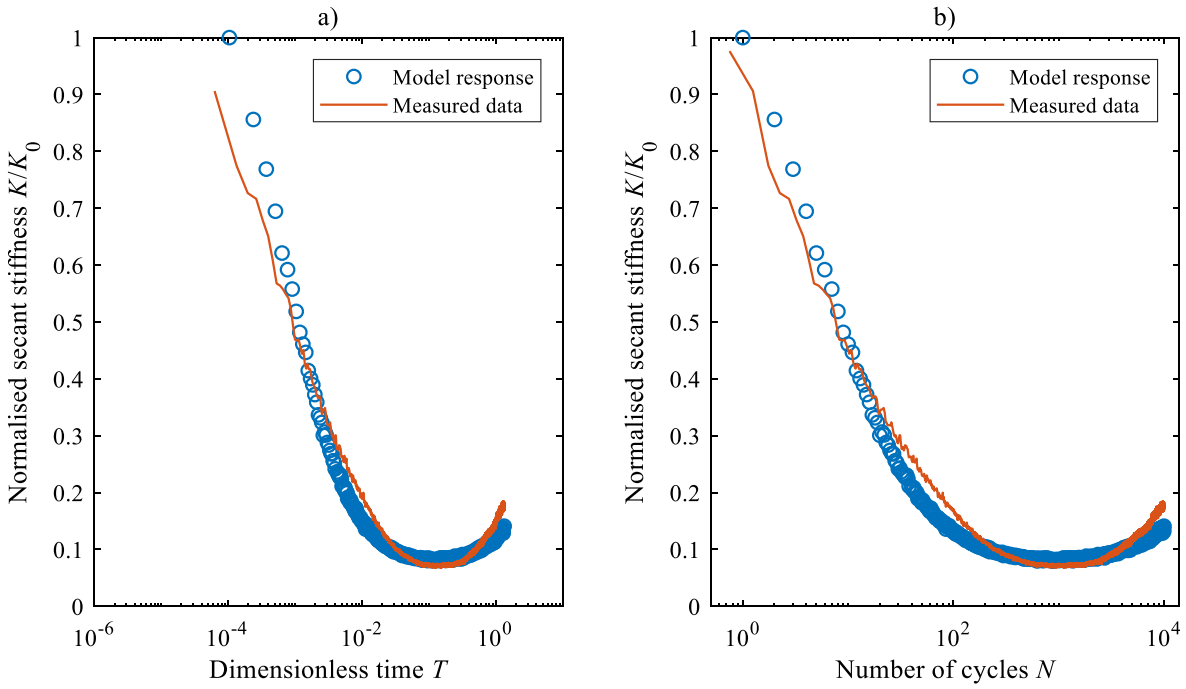

Fig. 13. Centrifuge test comparison: evolution of measured and computed stiffness vs a) dimensionless time T, b) Number of cycles.

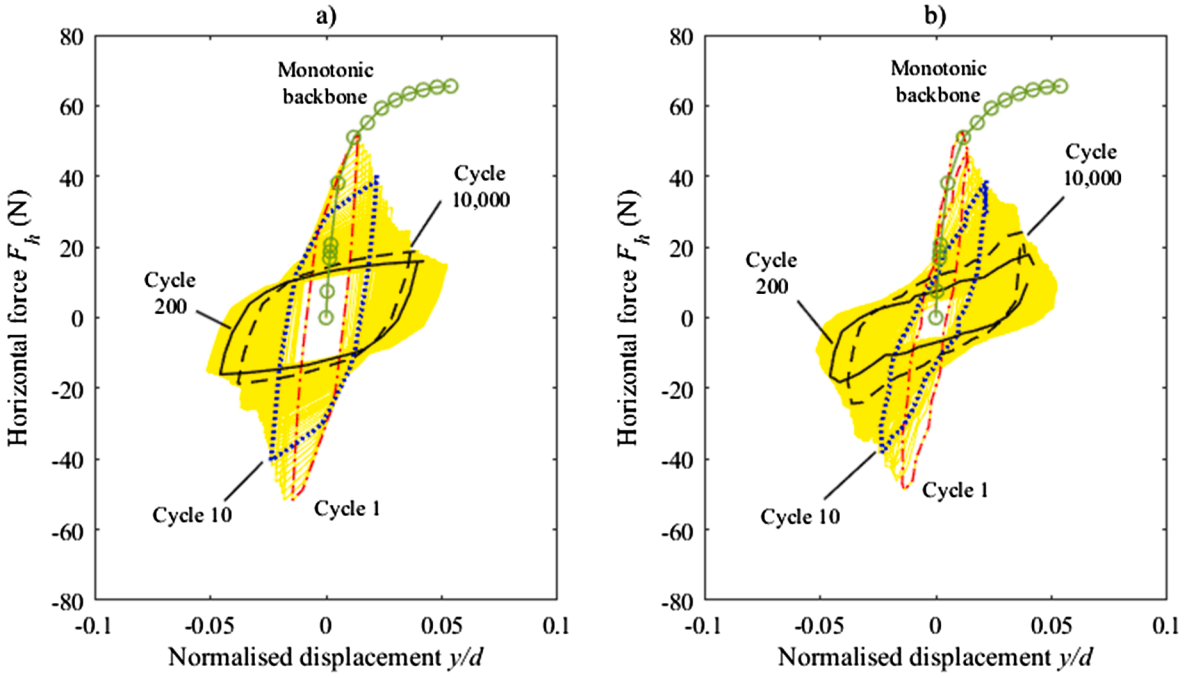

Fig. 14. Centrifuge test comparison: a) the calculated lateral response using PICSI b) measured response.

for cyclic modelling of piles and conductors (e.g. Whyte et al. 2020), and the PICSI model provides an overlay that captures soil softening and consolidation. This opens up the possibility of efficiently modelling the full 'whole life' history of changing soil support. This may unlock beneficial effects such as 'smearing' of fatigue damage as hot spots migrate along the pile, or a gain in pile capacity for life extensions. It may also provide a basis to interpret changes in system natural period that are observed as a result of evolving pile head stiffness. The model can be implemented within finite element lateral pile analysis software, and the changing strength (CSI) aspect could equally be overlain on other p-y models.

Some model parameters can be derived from conventional soil properties, although others may require alternative methods of calibration. Methods exist to scale the soil stress:strain response seen in direct simple shear (DSS) tests directly to the monotonic *p-y* response (Zhang and Andersen 2017), and extensions to cyclic behaviour have been proposed (Erbrich et al. 2010, Zhang et al. 2017). The same approach could be used to calibrate the PICSI model parameters from DSS responses, or alternatively the *p-y* element test described by (Zakeri et al. 2017) could provide a more direct calibration. The combined effects of softening and consolidation are not usually considered in a single soil element test or a conventional in situ test. However, 'episodic'

versions of both the T-bar (White and Hodder 2010, Zhou et al. 2020) and the DSS test (Yasuhara & Andersen 1991, Truong et al. 2019, Laham et al., 2021) are possible, and offer the potential to provide model parameters by measuring responses akin to Fig. 6.

The PICSI model has been developed with soft soils in mind, which lie initially on the 'wet' side of the critical state line and therefore show a tendency to contract under loading, generating positive excess pore pressure. Under cyclic loading, even soils that have been over-consolidated to an over-consolidation ratio (OCR) value that places them slightly on the 'dry' side of the CSL tend to generate positive pore pressure under cyclic loading (e.g. Andersen 2015), so the model may work well even for these higher OCR soils. It is also possible to conceive a reflected version of the model framework (Fig. 1) in which the soil moves up the vertical axis, softening rather than hardening, which could represent soils that are initially dilatant and generate negative excess pore pressure, which leads to swelling and softening after dissipation. However, at present, we have not attempted to consider such high OCR cases, and we have focused instead on soft soils, where the opposing effects of cyclic softening and consolidation hardening are topical and offer potential design optimisation in relation to 'whole life design' (e.g. Lai et al. 2020, Laham et al. 2021, Gourvenec 2020, Guevara et al. 2020).

6. Concluding comments

This paper sets out a new *p-y* model for the long term 'whole life' behaviour of laterally-loaded piles in soft clay. It addresses an emerging requirement to capture the progressive changes in soil support that occur in soft soils around piles and well conductors, which influence the capacity, stiffness and fatigue of these systems.

The model is inspired by model testing observations and theoretical solutions for each element of the behaviour, and combines a parallel-Iwan (PI) non-linear spring with a critical state-inspired overlay for the changing strength and stiffness. It allows the general responses observed in model tests to be replicated, with many parameters being fixed based on theoretical considerations. A new efficient methodology for defining the PI sub-springs is set out.

This new basis for whole life modelling of piles and well conductors, allowing changes in stiffness and capacity to be simulated, may lead to beneficial improvements in predictions of system stiffness, fatigue and late-life capacity.

CRediT authorship contribution statement

D.J. White: Conceptualization, Methodology, Software, Writing – original draft. **J.P. Doherty:** Conceptualization, Methodology, Software, Writing – original draft. **M. Guevara:** Investigation, Writing – review & editing. **P.G. Watson:** Supervision, Writing – review & editing, Funding acquisition.

Declaration of Competing Interest

The authors declare that they have no known competing financial interests or personal relationships that could have appeared to influence the work reported in this paper.

Acknowledgements

This work is part of the activities of the ARC Industrial Transformation Research Hub in Offshore Floating Facilities (the OFFshore Hub, www.offshorehub.edu.au), which is funded by the Australian Research Council, Shell, Woodside, Lloyds Register and Bureau Veritas (ARC grant IH140100012). The first and fourth authors also acknowledge support from the Shell Chair in Offshore Engineering at UWA, which is sponsored by Shell Australia. The first author also acknowledges support from the UK EPSRC Offshore Renewable Energy Supergen Hub (EPSRC grant EP/S000747/1).

References

Andersen, K.H., 2015. Cyclic soil parameters for offshore foundation design. The 3rd ISSMGE McClelland Lecture. In: Meyer (Ed.), Frontiers in Offshore Geotechnics III, ISFOG'2015. Taylor & Francis Group, London. ISBN: 978-1-138-02848-7. Proc., pp. 5–82. Revised version in: http://www.issmge.org/committees/technical-committees/applications/offshoreand.

Andersen, K.H., Kleven, A., Heien, D., 1988. Cyclic soil data for design of gravity structures. ASCE J. Geotech. Eng. 114 (5), 517–539.

API (American Petroleum Institute), 2011. Geotechnical and foundation design considerations, API recommended practice RP2GEO, first ed. API, Washington, DC, USA.

Baguelin, F., Frank, R., Saïd, Y.H., 1977. Theoretical study of lateral reaction mechanism of piles. Géotechnique 27 (3), 405–434.

Beuckelaers, W.J.A.P., 2015. Fatigue life calculation of monopiles for offshore wind turbines using a kinematic hardening soil model. In: Proceedings of the 24th European Young Geotechnical Engineering Conference (EYGEC), 1–5. Durham. pp. 1–5.

Boukpeti, N., White, D.J., 2017. Interface shear box tests for assessing axial pipe-soil resistance. Géotechnique 67 (1), 18–30.

Cocjin, M.L., Gourvenec, S.M., White, D.J., Randolph, M.F., 2014. Tolerably mobile subsea foundations – observations of performance. Géotechnique 64 (11), 895–909.

Cocjin, M.L., Gourvenec, S.M., White, D.J., Randolph, M.F., 2017. Theoretical framework for predicting the response of tolerably mobile subsea installations. Géotechnique 67 (7), 608–620.

DNV-GL, 2019. RP-C212 Offshore soil mechanics and geotechnical engineering. Recommended Practice. DNV-GL.

Doherty, J., White, D.J., Watson, P.G., and Grime, A., 2019. Life cycle changes in p-y stiffness for a conductor pile installed in carbonate silt. In: Proceedings of the 1st Vietnam symposium on advances in offshore engineering: VSOE 2018. Lecture notes in civil engineering 18. Springer, Singapore. pp. 362–368.

Doyle, E.H., Sharma, J.S., Bolton, M.D., Valsangkar, A.J., Newlin, J.A., 2004. Centrifuge model tests on anchor piles for tension leg platforms. In: Proceedings of the Annual Offshore Technology Conference, Houston. OTC-16845.

Einav, I., 2005. Energy and variational principles for piles in dissipative soil. Géotechnique 55 (7), 515–525.

Erbrich, C.T., O'Neill, M.P., Clancy, P., Randolph, M.F., 2010. Keynote Lecture: Axial and lateral pile design in carbonate soils. In: Proceedings of the 2nd International Symposium on Frontiers in Offshore Geotechnics ISFOG 2010, Perth. pp. 125–154.

Gourvenec, S.M., 2020. Whole-life geotechnical design: What is it? What's it for? So what? And what next? Keynote. In: Westgate, Z. (Ed.), Proceedings 4th International Symposium on Frontiers in Offshore Geotechnics ISFOG 2020. Deep Foundations Institute, Austin, pp. 206–246.

Guevara, M., Doherty, J., Watson, P., White, D., 2020. Key features impacting soil-conductor lateral behaviour as illustrated by centrifuge tests. In: Proceedings of the 4th International Symposium on Frontiers in Offshore Geotechnics ISFOG 2020, Austin. pp. 1–10.

Hodder, M.S., White, D.J., Cassidy, M.J., 2009. Effect of remolding and reconsolidation on the touchdown stiffness of a steel catenary riser: Observations from centrifuge modeling. In: Proceedings of the Annual Offshore Technology Conference, Houston. OTC-19871.

Houlsby, G.T., Abadie, C.N., Beuckelaers, W.J.A.P., Byrne, B.W., 2017. A model for nonlinear hysteretic and ratcheting behaviour. Int. J. Solids Struct. 120, 67–80.

ISO, 2016. Petroleum and natural gas industries — Specific requirements for offshore structures — Part 4: Geotechnical and foundation design considerations. ISO 19901-4:2016, International Standards Organization, Geneva.

Iwan, W.D., 1966. A distributed-element model for hysteresis and its steady-state dynamic response. ASME. J. Appl. Mech. 33 (4), 893–900.

Jeanjean, P., Zhang, Y., Zakeri, A., Andersen, K.H., Gilbert, R., Senanayake, A., 2017. A framework for monotonic p-y curves in clay. In: Proceedings of the 8th International Conference of Offshore Site Investigation and Geotechnics, London. pp. 108–141.

Komolafe, O., Aubeny, C., 2020. A p-y analysis of laterally loaded offshore-well conductors and piles installed in normally consolidated to lightly overconsolidated clays. J. Geotech. Geoenviron. Eng. 146 (6), 1–18.

Lai, Y., Wang, L., Hong, Y., He, B., 2020. Centrifuge modeling of the cyclic lateral behavior of large-diameter monopiles in soft clay: effects of episodic cycling and reconsolidation. Ocean Eng. 200, 1–17.

Laham, N., Kwa, K., White, D.J., Gourvenec, S.M., 2021. Episodic direct simple shear tests to measure changing strength for whole-life geotechnical design. Geotech. Lett. 11 (1), 103–111.

Matlock, H., 1970. Correlations for design of laterally loaded piles in soft clay. In: Proceedings of the 2nd Annual Offshore Technology Conference, Dallas. OTC-1204. pp. 577–594.

Osman, A.S., Randolph, M.F., 2012. Analytical solution for the consolidation around a laterally loaded pile. Int. J. Geomech. 12 (3), 199–208.

Randolph, M.F., 2004. Characterisation of soft sediments for offshore applications. In: Proceedings of the 2nd International Conference on Site Characterization, Millpress Science, Porto. pp. 209–232.

Randolph, M.F., Houlsby, G.T., 1984. Limiting pressure on a circular pile loaded laterally in cohesive soil. Géotechnique 34 (4), 613–623.

Smith, V.B., White, D.J., 2014. Volumetric hardening in axial pipe soil interaction. In: Proceedings of the Annual Offshore Technology Conference Asia, Kuala Lumpur. OTC-24856.

Stewart, D.P., Randolph, M.F., 1991. A new site investigation tool for the centrifuge. In: Proceedings of the International Conference on Centrifuge Modelling, Centrifuge '91, Balkema, Rotterland. pp. 531–538.

Truong, P., Lehane, B.M., Zania, V., Klinkvort, R.T., 2019. Empirical approach based on centrifuge testing for cyclic deformations of laterally loaded piles in sand. Géotechnique 69 (2), 133–145.
White, D.J., Hodder, M., 2010. A simple model for the effect on soil strength of episodes of remoulding and reconsolidation. Can. Geotech. J. 47 (7), 821–826.
Whyte, S.A., Burd, H.J., Martin, C.M., Rattley, M.J., 2020. Formulation and implementation of a practical multi-surface soil plasticity model. Comput. Geotechn. 117, 1–18.
Wroth, C.P., Wood, D.M., 1978. The correlation of index properties with some basic engineering properties of soils. Can. Geotech. J. 15 (2), 137–145.
Yasuhara, K., Andersen, K.H., 1991. Recompression of normally consolidated clay after cyclic loading. Soils Found. 31 (1), 83–94.
Zakeri, A., Sturm, H., Dyvik, R., Jeanjean, P., 2017. Development of novel apparatus to obtain soil resistance–displacement relationship for well conductor fatigue analysis. Can. Geotech. J. 54 (10), 1435–1446.
Zhang, C., White, D., Randolph, M., 2011. Centrifuge modeling of the cyclic lateral response of a rigid pile in soft clay. J. Geotechn. Geoenviron. Eng. 137 (7), 717–729.
Zhang, Y., Andersen, K.H., 2017. Scaling of lateral pile p-y response in clay from laboratory stress-strain curves. Mar. Struct. 53, 124–135.
Zhang, Y., Andersen, K.H., Jeanjean, P., Mirdamadi, A., Gundersen, A.S., Jostad, H.P., 2017. A framework for cyclic p-y curves in clay and application to pile design in GoM. In: Offshore Site Investigation Geotechnics 8th International Conference Proceedings, Vol. 34, London. pp. 108–141.
Zhou, H., Randolph, M.F., 2009. Numerical investigations into cycling of full-flow penetrometers in soft clay. Géotechnique 59 (10), 801–812.
Zhou, Z., White, D.J., O'Loughlin, C.D., 2020. The changing strength of carbonate silt: parallel penetrometer and foundation tests with cyclic loading and reconsolidation periods. Can. Geotech. J. 57 (11), 1664–1683.